The Roles of Langmuir Circulations in the Dispersion of Surface Tracers

ALAN J. FALLER

Institute for Physical Science and Technology, University of Maryland, College Park, Maryland

STEPHEN J. AUER

NOAA, National Environmental Satellite, Data, and Information Service, Suitland, Maryland

(Manuscript received 11 May 1987, in final form 29 December 1987)

ABSTRACT

A hierarchy of theoretical and numerical models for the dispersion of discrete floating tracers on lakes and oceans is presented. Central to these models is the role of Langmuir circulations, which concentrate tracers into narrow windrows thus inhibiting tracer dispersion. But time-dependent Langmuir circulations cause the rows of tracers to wander and to split, by local time dependence and by downwind advection, thus promoting dispersion. Accordingly, the Langmuir circulations generally render the smaller-scale background turbulence irrelevant for direct estimates of surface dispersion.

Analytical models include: 1) a theory of tracers in a linear mean-flow convergence plus homogeneous turbulence, this theory being applicable to the width of windrows; and 2) a model with a spatially periodic mean flow and a periodic small-scale eddy diffusion coefficient that allows an estimate of the Langmuir-scale dispersivity for steady parallel cells.

Random-flight calculations for a model of complex time-dependent and downwind dependent Langmuir circulations have led to the explicit prediction $K^* = 0.5T_c^{*-1/2}$ where K^* and T_c^* are the nondimensional dispersivity and cellular time scale, respectively.

1. Introduction

The dispersion of floating material on lakes and oceans can be caused by many scales of motion. At least since Richardson (1926) it has been recognized that the growth in size of a cloud of tracers with the characteristic dimension σ depends primarily upon turbulent scales of roughly the same dimension as the cloud, if such scales exist. For a full spectrum of turbulent scales encompassing σ, very much larger scales simply advect the cloud as a body and scales much less than σ act as a small-scale Fickian diffusion. Okubo (1971) has summarized many observational studies of oceanic dispersion, but in general those measurements were concerned with scales of motion much larger than those treated here.

In addition to irregular motions characterized as turbulence, however, there are organized flows such as those associated with fronts, mesoscale eddies, nearshore topographic features, etc. that may be nearly steady on the time scale of any particular cloud of tracers. If we have detailed knowledge of these flows they can be taken into account explicitly as prescribed flows. As our knowledge of natural processes assumes greater detail, more of what was once called turbulence will be assigned to these prescribed flows.

Surface motions in lakes and oceans up to a few hundred meters in scale are often dominated by the quasi-steady phenomenon known as Langmuir circulation. Langmuir circulations (LCs) consist of a series of roll vortices of alternating sign of rotation with horizontal axes more or less parallel to the wind. These circulations were first systematically investigated by Irving Langmuir (1938) who attributed mixed layers largely to the overturning produced by these wind-driven circulations. Their surface manifestation is generally a pattern of windrows: bands of surface film, foam, debris, etc. at the lines of horizontal surface convergence between rolls. But LCs often may be present without visual indicators to mark their locations. In natural settings the windrows may adopt a pattern of "venous streaks" or "parallel streaks" (Stommel 1951) (Fig. 1), the latter being favored by steady winds and, in lakes, by a shallow flat bottom; and the former occurring with gusty winds and other disturbing factors. While most observations of windrows have relied upon visible tracers, McLeish (1968) has clearly shown that a similar streakiness of the ocean surface is also often evident in very sensitive infrared photographs of the pattern of sea-surface temperature.

An excellent review of the Craik-Leibovich theory of LCs (a wave/shear interaction that appears to be

Corresponding author address: Professor Alan J. Faller, Institute for Physical Science and Technology, University of Maryland, College Park, MD 20742.

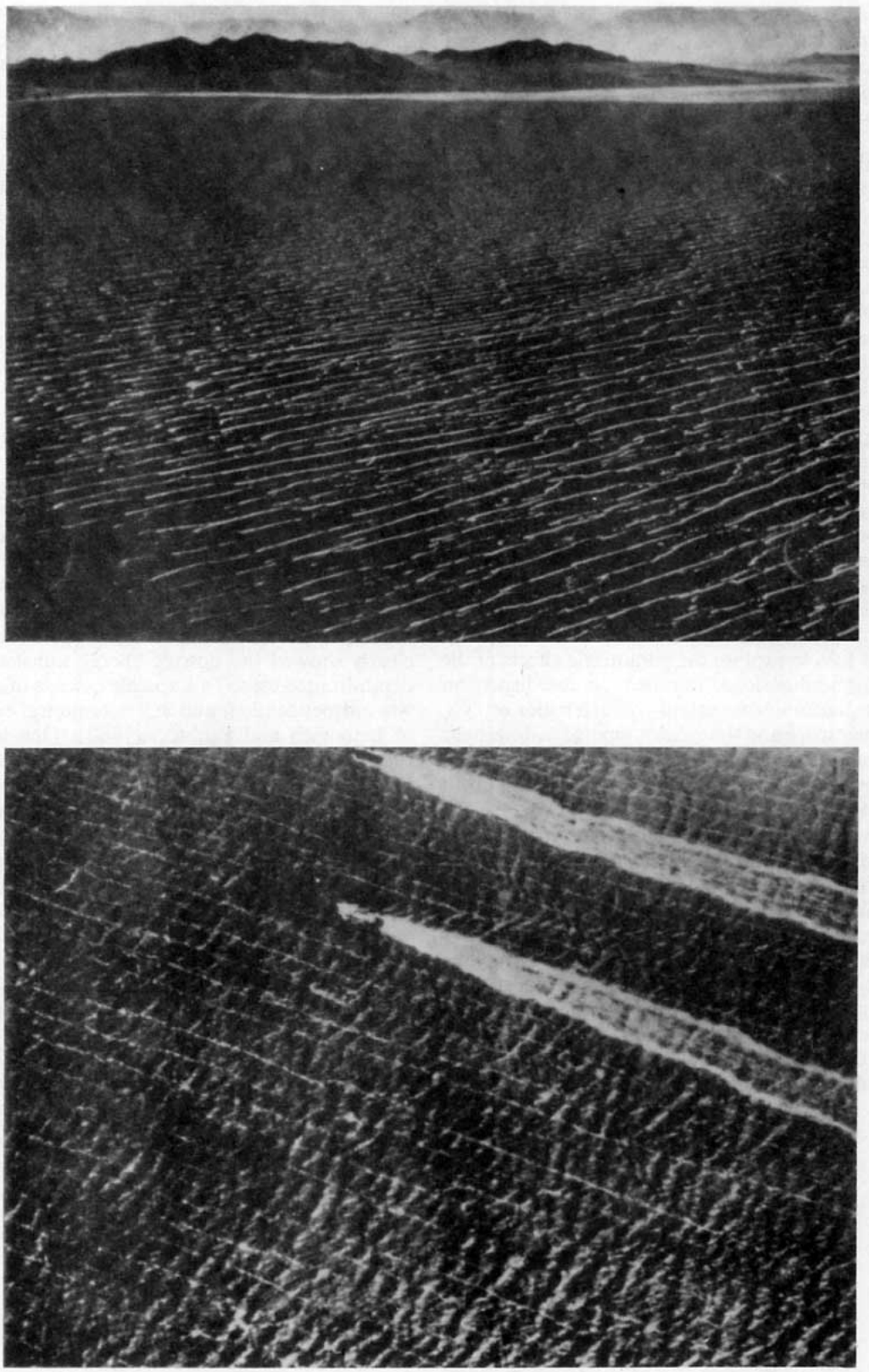

FIG. 1. Examples of venous and parallel streaks, reprinted from Weather (Stommel 1951). Original photographs were by Prof. A. J. Eardley, University of Utah, on Great Salt Lake (upper), and by Mr. Alfred H. Woodcock, Woods Hole Oceanographic Institution, on the Banana River, Florida (lower).

the primary mechanism) and many of the observational studies has been provided by Leibovich (1983). In the meantime, recent measurements by Weller et al. (1985) and Smith et al. (1987) have provided the first instrumented observations of large vertical velocities deep in the mixed layer that unambiguously demonstrate the large depth of penetration of LCs. These confirm and add much detail to the earlier indirect observations of Woodcock (1950), Johnson and Richardson (1977), and others that have supported Langmuir's contentions regarding the importance of these circulations in the dynamics of mixed layers in the ocean. Observations by Scott et al. (1969), Myer (1971), and Filatov et al. (1981) have clearly demonstrated the importance of LCs for mixed layers of lesser depth in lakes.

Here we are concerned with the effects of LCs primarily upon the lateral (across wind) dispersion of floating tracers. On the one hand, this presentation is a study of surface dispersion. On the other, it may be viewed in terms of the question: How much can we learn about mixed-layer dynamics by the study of surface tracers? The LCs will be treated as a prescribed flow, in some cases as time dependent, with a superimposed small-scale turbulence. We systematically develop a hierarchy of analytical and numerical idealizations of LCs to explore the parametric effects of the relevant nondimensional numbers on the dispersion of tracers. Inasmuch as certain characteristics of LCs, such as their space and time scales, emerge as dominant factors for surface dispersion, we now briefly review some characteristics of LCs that are important for our development of the subject.

Langmuir circulations may have spatial scales from a few centimeters (with capillary waves, as in Faller and Caponi 1978, hereafter FC); and beneath surface films, as in Faller and Perini 1984) to greater than 100 m (Langmuir 1938; Smith et al. 1987). Laboratory experiments (Faller 1969; FC) have shown that when the lower boundary is a controlling factor the spacing of the largest cells is normally in the range $2.5 < L/H < 3.5$, where L is the crosswind wave length of the cells and H is the depth of the fluid or perhaps the depth of the mixed layer. Similar results were independently obtained by Buranathanitt and Cockrell (1979) in laboratory studies designed to simulate the effects of LCs upon particle motions in lakes and reservoirs. This conclusion with respect to the limiting effect of the bottom boundary for the largest cells has been confirmed in the ocean by the recent Doppler SONAR observations from *FLIP* in MILDEX by Smith et al. (1987) who found the ratio $L/H = 3$, the ratio staying nearly constant while H increased (tidally) from 40 to 60 m. This effect of the bottom would at first seem to be at variance with the observations of Faller and Woodcock (1964) and others, namely that wind speed is an important factor in determining L, as well as appearing to be at odds with the Craik-Leibovich mechanisms of wave/shear generation (Craik and Leibovich 1966; Craik 1977). But the effect can readily be explained in terms of the cascade of energy from smaller to larger scales, an important characteristic of two-dimensional turbulence that appears to operate with these nearly two-dimensional rolls.

Many observers (e.g., Williams 1965; Assaf et al. 1971) have found that several scales of LCs may exist simultaneously. Laboratory experiments (FC) showed that when wind-wave generated LCs first form, their scale is generally smaller than the cells that dominate the flow at a later time. Vane-generated rolls (FC) also clearly showed the upscale energy transfer to larger, depth-limited cells. This upscale cascade of energy also was independently found in the numerical experiments of Leibovich and Paolucci (1980). One infers from these results that in nature the smaller scales may be the direct result of wave/shear generation and have a scale L_0 related to the dominant scale of gravity waves and perhaps related to the depth of the layer of high shear near the surface. The depth-limited scales with $L \approx 3H$, however, appear to be a consequence of upscale energy transfer, with the exception of those cases, of course, where L_0 is already close to, or greater than, $3H$. Figure 2 illustrates the concept of continuously generated small vortices and their accumulation into larger, depth-limited, and less rapidly changing cells.

The possibility of this important upscale energy transfer was first suggested to one of us (Faller) during conversations in Woods Hole (circa 1963) by E. R.

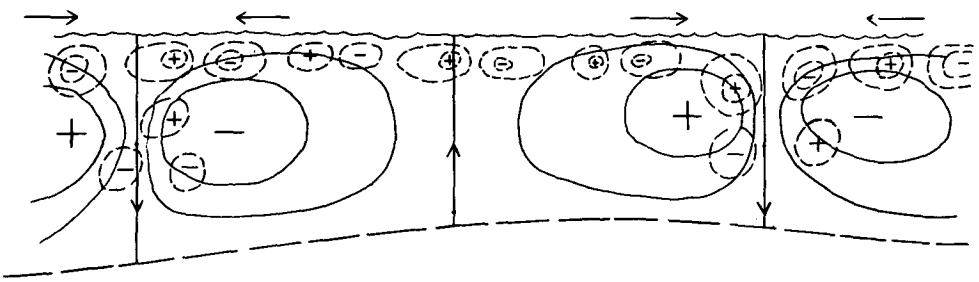

FIG. 2. A sketch of the superposition of smaller-scale and larger-scale Langmuir circulations, the former being driven directly by wave–shear interaction and the latter generated by an upward cascade of energy from smaller scales.

Baylor on the basis of observations at sea. Baylor was one of the early investigators of the effects of LCs upon biological processes, and it was in one of his publications (Sutcliffe et al. 1963) that the term "Langmuir circulation" was first adopted.

The t-(time) dependence and x-(along wind) dependence of LCs both seem to be important factors for dispersion and appear to be closely related. The smaller LCs, those directly generated by wave/shear mechanisms, are likely to be subject to time and space variations of the wind because of their lesser inertia. Thus, as observed by Stommel (1952), small windrows respond rapidly to gusty winds. Accordingly, and noting Fig. 2, one should expect: 1) t- and x-dependence of the small scales in relation to the gustiness of the wind; 2) a drift of these scales to both the left and right of the wind direction (relative to any mean drift of the mixed layer); 3) stochastic forcing of the largest scales; and 4) t- and x-dependence of the largest scales, perhaps more or less in proportion to that of the small scales.

The characteristic time scale of LCs, T_C, may depend upon several factors: lateral scale, depth of penetration, time scale of the wind, undulations of the mixed layer depth, and possible hydrodynamic instabilities of well-developed LCs themselves. Parallel streaks (and rolls) probably occur only for steady winds and perhaps they require a well-defined shallow bottom, as well. Then T_C can be considered to be essentially infinite, (excepting slow changes of the weather) as in many of the observations of Kenney (1977) in shallow, flat-bottomed lakes. But under the stochastic forcing conditions that may occur in the ocean, what is the value of T_c to be expected? In appendix A, we identify a minimum T_c with the characteristic response time of LCs, T_R, to an abrupt change of forcing. We then enlist a set of somewhat disparate natural and laboratory estimates of T_R that suggest the formula $T_R = L/(0.03\ \text{m s}^{-1})$ (see Fig. 3). Imperfect as this result may be, some such estimate is required in later sections, and so we adopt the relation $T_c = L/(0.03\ \text{s}^{-1})$.

McLeish (1968) discussed many of the qualitative effects to be expected from organized turbulent motions acting on tracers confined to the free surface, but Csanady (1974) was the first to quantitatively discuss the larger-scale dispersion of surface tracers due to LCs. For certain conditions on Lake Huron, he estimated an effective surface eddy-diffusion coefficient of $K = 10^3\ \text{cm}^2\ \text{s}^{-1}$. This estimate was based on a length scale L (10^3 cm) and a time scale T_C (10^3 s), values that seemed appropriate to a variety of observations. The value of K was determined simply from $K = L^2/T_C$, and was, at least in order of magnitude, in agreement with the results of earlier dye-dispersion studies (Csanady 1970). His description of the dispersive effect was "as a cloud [of discrete floating tracers] is released it rapidly forms itself into a number of windrows. Given a typical lifetime of 10^3 s each windrow acts as a new source with about this frequency, redistributing its load over a few successor windrows".

In view of the wide variability of natural conditions, estimates of the above type may be all that can be expected to describe the gross effects of LCs at the present time. Nevertheless, it is interesting and perhaps worthwhile to speculate on further details of the effects of LCs on the motions of surface tracers with the expectation of obtaining better estimates of K and other characteristics of the problem. Indeed, as appealing as the above row-splitting argument may seem, it will be

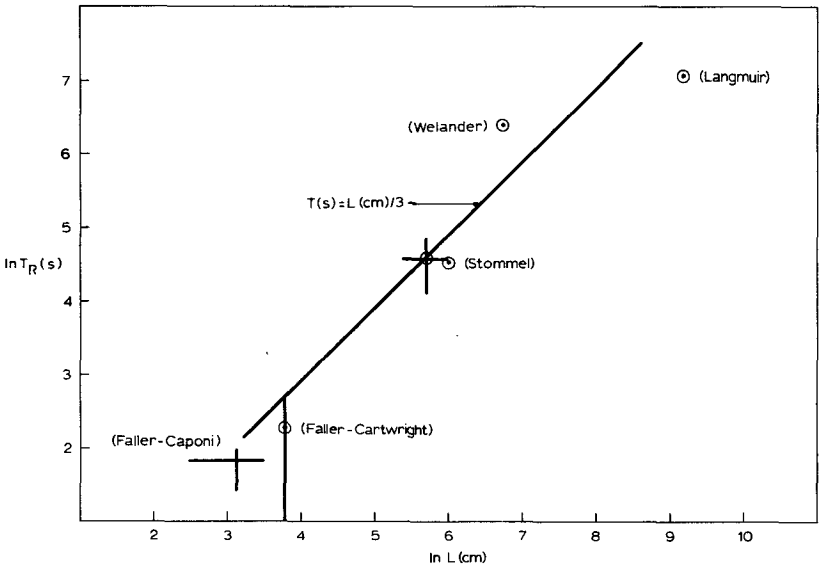

FIG. 3. Estimates of the time scales of Langmuir circulations with uncertainty bars as appropriate, for a large range of spatial scales.

found that our models indicate that row-splitting should occur infrequently and that the principle mechanism of dispersion is the stochastic wandering of rows in time and space, somewhat like a random walk and with $K \approx T_c^{-1/2}$.

2. A linear convergence model, nondimensional numbers, and "standard values"

It is to be expected that when LCs are strong relative to the turbulence, floating tracers will become concentrated in narrow bands (windrows) at the convergence lines. In the vicinity of these narrow bands one can consider the mean flow to be linear in y, the crosswind direction. Thus in the simple periodic case with

$$\tilde{v} = -V \sin ky, \tag{1}$$

close to the convergence line at $y = 0$ the mean flow $\tilde{v}$ can be approximated by

$$\partial \tilde{v}/\partial y = -Vk. \tag{2}$$

Analytical solutions for the distribution of tracers with this mean flow and with a superimposed homogeneous turbulence were developed in Faller and Mignerey (1982, hereafter FM) and some of the basic results are reviewed here for their relevance to our problem.

Let the linear mean flow be $\tilde{v} = -Ay$ where $A = \partial \tilde{v}/\partial y$ is constant. Then from FM the steady-state distribution of tracers about $y = 0$, as specified by the tracer variance, is

$$\overline{y^2} = \overline{v^2} A T_l / A^2 (1 + AT_l) \tag{3}$$

where $\overline{v^2}$ is the mean square turbulent velocity component along y and T_l is the Lagrangian time scale of the turbulence. This result can be found by 1) assuming a turbulent velocity autocorrelation $\overline{v(t)v(t+\tau)}/\overline{v^2} = \exp(-\tau/T_l)$ to allow explicit integration, 2) integrating the equation $dy/dt = -Ay + v(t)$ to obtain $y(t)$ for an individual tracer, 3) squaring and taking an ensemble average to obtain a general expression for $\overline{y^2}(t)$, and 4) taking the limit of large t. Thus (3) is an exact analytical, steady-state solution that takes into account the separate effects of v and T_l but contains the assumption of an exponentially decaying autocorrelation function for v.

The corresponding eddy-diffusivity solution (FM) is

$$\overline{y^2} = D/A \tag{4}$$

where $D = \overline{v^2} T_l$ is the eddy diffusivity. Thus (4) differs from (3) by the factor $(1 + AT_l)$, and the significance of this difference rests on the magnitude of the nondimensional number AT_l. Random flight computations (section 4) have verified (3) and shown, in addition, that the distribution of tracers about $y = 0$ is Gaussian.

As a possible example of the use of (3), consider the distribution of *Sargassum* in the subtropical convergence zone of the North Atlantic Ocean due to the Ekman drift from the north and from the south. Estimating A to be 0.1 m s^{-1}/1000 km ($A = 10^{-7}$ s^{-1}) and letting the turbulence parameters be $\overline{v^2} = 0.10$ m^2 s^{-2} and $T_l = 20 \times 10^5$ s (for Rossby waves propagating through the region), one finds $AT_l = 0.2$ and $\overline{y^2}^{1/2} = 400$ km, the standard deviation of spread of the accumulated *Sargassum*. This is a reasonable estimate of the north–south distribution of *Sargassum* which "covers an oval measuring 1000 miles by 2000 miles" (Cowen 1960). Note that the value of AT_l is on the verge of being an important correction to the diffusion solution, but with the uncertainties of our estimates and the omission of recirculation patterns and other processes this is a moot point.

In the periodic case governed by (1), near $y = 0$ the combination AT_l becomes $VkT_l = T_l^*$, denoting nondimensional numbers by asterisks. T_l^* is one of three independent nondimensional numbers that can be formed from the five dimensional variates V, v, k, T_l and T_C. Our other two nondimensional numbers will be $v^* = \overline{v^2}^{1/2}/V$, and $T_c^* = VkT_c$. Lengths, velocities and times are scaled by k^{-1}, V, and $T_V = (Vk)^{-1}$, respectively. The latter factor, T_V, can be viewed as the overturning or advective time scale of the cells, not to be confused with T_C which involves time-dependence of the cell pattern. The combination $D^* = Dk/V = v^{*2} T_l^*$ is the nondimensional eddy diffusion coefficient.

It should be noted that a diffusion solution makes no distinction between the separate effects of v and T_l and may be thought of as the limiting case of finite D but with $T_l \to 0$. Thus, in the case of linear $\tilde{v}$ the diffusion result in (4) corresponds to $AT_l \to 0$ in (3) and in the periodic case it corresponds to $T_l^* \to 0$. Random flight calculations, however, explicitly include the effects of a finite T_l. As a general rule we refer to the spread of tracers in time as diffusion only in reference to small-scale turbulent effects. Otherwise the spread of tracers will be referred to as dispersion.

In later sections it is desirable to make estimates of oceanic dispersion and for this purpose we adopt "standard values" of the independent parameters. These are $V = 0.10$ m s^{-1}, $L = 37.7$ m ($k = 0.17$ m^{-1}), $\overline{v^2}^{1/2} = 0.04$ m s^{-1}, $T_l = 6$ s, and $T_C = 20$ min. It follows that $D = 0.0096$ m^2 s^{-1}. We also take $U_w = 0.30$ m s^{-1} as the downwind speed of tracers in a windrow. These values have been chosen in part to represent what we believe to be a typical set of oceanic conditions and in part to give the convenient nondimensional numbers $T_l^* = 0.10$, $T_c^* = 20$, $v^* = 0.4$, and, therefore, $D^* = 0.016$.

3. An analytical model for steady, periodic cells

This analysis assumes a pattern of free-surface convergence and divergence due to steady and spatially

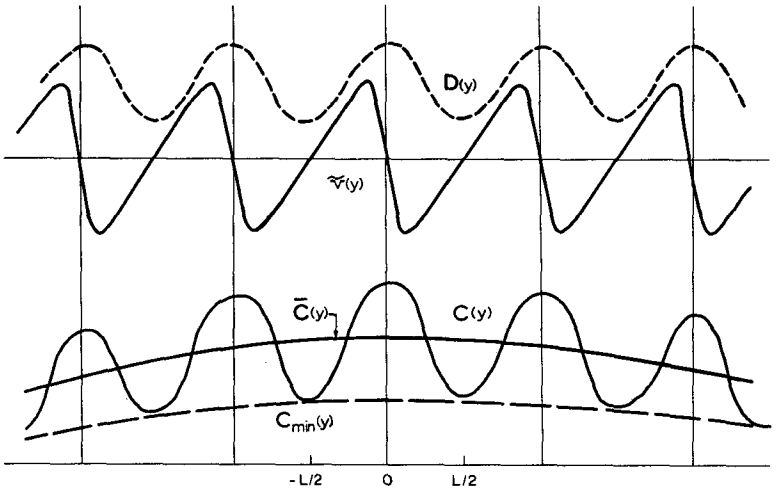

FIG. 4. An illustration of the periodic spatial variation of variates for the analytical diffusion model of section 3.

periodic two-dimensional LCs. A spatially variable eddy diffusivity patterned in relation to the mean flow (in a manner to be explained) also is allowed. While this model permits estimates of dispersion only for this idealization, it also serves as a base for the test of random-flight calculations that must be used in those more involved situations where analytical solutions are not available.

Consider a periodic mean flow $\tilde{v}(y)$ and a corresponding eddy diffusivity $D(y)$. The repetition length is L and the dominant wavenumber is $k = 2\pi/L$. As shown in Fig. 4 a convergence line is assumed to lie at $y = 0$, and therefore $\tilde{v}$ is an odd function of y, expressible as a sine series. In turn D should be symmetrical with respect to a convergence line (Fig. 4) and must be an even function of y, expressible as a cosine series.

The one-dimensional advection-diffusion equation is

$$\partial C/\partial t + \partial(\tilde{v}C)/\partial y = \partial(D\partial C/\partial y)/\partial y \qquad (6)$$

where C is the concentration of tracers per unit length crosswind. A cloud of tracers with standard deviation σ is assumed to span many cells, hence $\sigma \gg L$. Within cells C is expected to have a small-scale variation that is essentially the same from one pair of cells to another, as in Fig. 4. But a running average of C with an averaging length L, as defined by

$$\bar{C} = \int_y^{y+L} C(y')dy'/L, \qquad (7)$$

produces the smooth curve $\bar{C}(y)$.

We seek the formulation of an effective dispersivity K that describes the spread of the large cloud of tracers due to the combined effects of the cells and the turbulence. The dispersion equation will be

$$\partial\bar{C}/\partial t = K\partial^2\bar{C}/\partial y^2. \qquad (8)$$

If the distribution of $\bar{C}$ were Gaussian with standard deviation σ it would follow that $\partial\sigma^2/\partial t = 2K$, but a Gaussian distribution is not used in the following analysis.

Any within-cell adjustments of C should take place in a short time $T_V = (Vk)^{-1}$ where V is now simply a representative magnitude of the mean flow, $\tilde{v}$. T_V will be much smaller than the dispersive time scale associated with (8), so after initial rapid adjustments of the tracers to the cells, C will change only slowly, with the same time scale as $\bar{C}$. Then in (6) there will be nearly a local balance of advective and diffusive terms with small $\partial C/\partial t$.

A solution for K is obtained essentially by a double integration of (8), making use of the small $\partial\bar{C}/\partial t$ and $\partial\bar{C}/\partial y$ and the fact that at $y = nL/2$ (n odd) $\tilde{v} = 0$. At these points the total flux is limited by the minimum values of D (see Fig. 4). Further details of the method may be found in Faller and Auer (1987). The solution is

$$K = 1/(\overline{e^{-F}}\,\overline{e^{F}/D}) \qquad (9)$$

where F is defined by

$$F \equiv -\int_0^y (\tilde{v}/D)dy \qquad (10)$$

and, as before, the bar is an average over one wavelength.

The solution (9) is of the same form as that which appears in the physics literature for the diffusion of Brownian particles in a periodic potential (e.g. Das 1979; Ryter 1982) although derived differently and in quite different notation. The exposition of Weaver (1979) illustrates a particularly interesting and completely different approach with the same result. The corresponding concentration of tracers is specified by

$$C(y) = C(0)e^{-F(y)}. \qquad (11)$$

In applying these results, note in particular the restriction that D and $\tilde{v}$ must be even and odd functions of y, respectively, as the problem is defined here. Therefore a non-zero average value of $\tilde{v}$, i.e., a mean flow $\tilde{v}$ across the cells, as might sometimes occur in nature, is not permitted in this model.

Some special cases of (9) serve to illustrate its application. For $\tilde{v} = -V \sin y^*$ and $D = \bar{D}(1 + \alpha \cos y^*)$ it follows that (10) can be integrated directly with the result

$$F = -\beta \ln(1 + \alpha \cos y^*) \tag{12}$$

where $\beta = V/k\bar{D}\alpha = (\bar{D}^*\alpha)^{-1}$. Then (9) becomes

$$K/\bar{D} = 1/\overline{(1 + \alpha \cos y^*)^{\beta}}\,\overline{(1 + \alpha \cos y^*)^{-(1+\beta)}} \tag{13}$$

which can be evaluated computationally. In the especially simple case $V = 0$, i.e. only a spatial variation of D, one finds

$$K/\bar{D} = 1/\overline{(1 + \alpha \cos y^*)^{-1}}. \tag{14}$$

When (14) is written as

$$1/K = \overline{1/D} \tag{15}$$

K will be recognized to be the harmonic mean of D.

Another example is the case $\alpha = 0$, i.e. $D = \bar{D}$. With the mean flow given by (1) the solution reduces to

$$K/D = 1/\{\overline{\exp[-D^{*-1}(1 - \cos y^*)]} \times \overline{\exp[D^{*-1}(1 - \cos y^*)]}\} \tag{16}$$

which is a function of only the single parameter D^*. Figure 5 illustrates K/D versus D^{*-1} from (16) and can be used to estimate the surface dispersion due to steady parallel cells. With our standard values (see section 2) $D^{*-1} = 62.5$, and it is apparent from Fig. 5 that the cells then completely dominate the turbulence and give, in effect, $K = 0$. Thus, theory verifies that we should expect surface tracers to be strongly concentrated in rows as is frequently observed.

The distribution that corresponds to (16) is

$$C = C(0) \exp[-D^{*-1}(1 - \cos y^*)], \tag{17}$$

and for small y^* the approximation is

$$C = C(0) \exp(-D^{*-1}k^2y^{*2}/2), \tag{18}$$

a Gaussian distribution with the standard deviation

$$\sigma_C^* = D^{*1/2}, \quad \sigma_C = (D/kV)^{1/2}. \tag{19}$$

In natural circumstances there are several factors that may cause tracer distributions in narrow windrows to be slightly different from (17) apart from t- and x-dependence of the cells. These factors include spatial variations of D, harmonics of $\tilde{v}$, wave oscillations, finite T_t, and surface films. The effects of a surface film will depend upon the nature of the tracers and of the film in subtle ways that we cannot consider here. Thus, we assume that significant films are not present or that the tracers are immersed a few centimeters into the water so that film effects can be neglected.

The wave oscillations of importance will be those normal to the windrows. Assuming a 10 m s^{-1} wind, the significant wave height would be about 2 m (Neumann and Pierson 1966). Then the standard deviation of tracer oscillation along the wind direction would be about 1 m and waves moving at 20 degrees to the windrow would produce a transverse oscillation of about 0.35 m. The wavelength of such waves, however, would be about 40 m, very long compared to the row width, and the waves would only bend the row slightly without causing local apparent dispersion. Waves that would directly affect the spread of tracers would be of

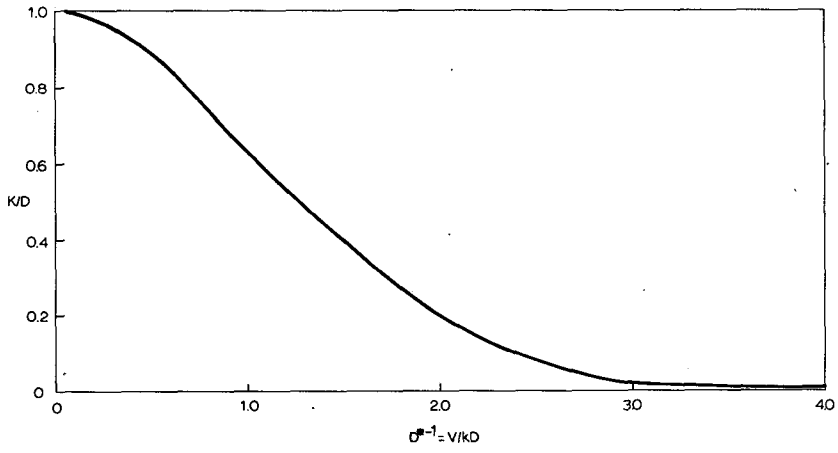

FIG. 5. The ratio of the large- and small-scale diffusion coefficients from the diffusion model of section 3 (ordinate) as a function of the inverse, nondimensional diffusion coefficient (abscissa). The value of D^{*-1} to be expected in lakes and oceans lies far off scale to the right thus implying that for steady parallel cells the large-scale diffusion is essentially zero.

about the same dimension as the row width. From (19) an estimate of the row width is $\sigma_C = 0.76$ m, but waves of comparable length would have negligible transverse oscillations.

Variations of D and harmonics of $\tilde{v}$ can be explicitly included in our model. At the free surface one should expect the turbulence to be strongest at the convergence lines, except perhaps for possible film effects, because water moving toward the windrows has been subjected to the wind stress and wave action for the longest time. At the divergences, upwelling brings up relatively calm water. These effects were very obvious from dyes and discrete tracers in laboratory experiments (Faller 1978) although turbulence levels were not directly measured. To examine the effect of variable D we have tried $\alpha = 0.9$ in (13) thus producing a spatial variation of D from $0.1\bar{D}$ to $1.9\bar{D}$.

Table 1 gives the ratios $2\sigma_C/L$ for several values of $\bar{D}^*$, where σ_C is the standard deviation of C within cells, i.e., for $-\pi < y^* < \pi$. This ratio is the relative (within-cell) spread of C. The maximum ratio is $2\sigma_C/L = 0.577$ which occurs for a uniform distribution of $C(V \to 0, D^* \to \infty)$. For small D^* we see from Table 1 that the spread (with $\alpha = 0.9$) was only $1.9^{1/2} = 1.38$ times that for $\alpha = 0$. This result also can be seen from the linear $\tilde{v}$ model of section 2 because for small D^* the tracers are concentrated near $y = 0$.

The effect of harmonics in $\tilde{v}$ is of the opposite sign from that due to variations of D and is of about the same magnitude. To see this let

$$\tilde{v} = -V \sin y^* - \frac{V}{2} \sin 2y^*, \tag{20}$$

the relative signs of the two components being consistent with the well-established concentration of downwelling beneath windrows as observed in nature. The chosen amplitude, $V/2$, of the first harmonic ($2k$) is based on the experiments of Faller and Cartwright (1983) and an interpretation of the response of surface tracers in other experiments (FC), and it doubles the rate of convergence at $y^* = 0$. From section 2 σ_C is reduced by 0.7071. Thus the effects of the assumed variations of D and harmonics of $\tilde{v}$ on the spread of tracers tend to cancel.

TABLE 1. The relative spread of tracers $2\sigma_C/L$ within windrows as a function of D^*. Column A is a spatially constant $D^* = \bar{D}^*$ and column B is for $D^* = \bar{D}^*(1 + 0.9 \cos y^*)$.

$D^{*-1} = \frac{V}{kD}$	A	B
0	.59	.59
0.5	.488	.458
1.0	.404	.374
2	.278	.284
4	.174	.207
10	.103	.156
20	.072	.097
50	.045	.062
100	.032	.044

The result (19) suggests the interesting possibility of estimating the relative strengths of the cells and of the turbulence by measuring the spread of large numbers of tracers in quasi-steady windrows. For example in the experiments of Faller and Cartwright (1983) where k was known and the values of V were measured, estimates of the spreads of tracers (plastic floats and paper dots) have shown that the turbulent diffusivities were in the range $0.25 < D < 1.8$ cm^2 s^{-1} for the various experiments.

The t- and x-dependence of naturally occurring cells are, of course, limiting factors for the study of windrow widths, but if T_C/T_V is large some rows will be quasi-steady and the theory can be judiciously applied. For our standard conditions $T_C/T_V = T_C^* = 20$.

4. The random-flight method

Random-flight calculations are correlated random walks of a large number of fluid tracers, a Monte-Carlo technique. The tracers are given an initial distribution in y characterized by some standard deviation σ. In time, due to the effects of the LCs and turbulence, the tracers disperse and σ increases. The dispersivity K is found from

$$d\sigma^2/dt = 2K. \tag{23}$$

The turbulent velocity component v_{im} for tracer i at time step m is calculated from the recursion relation

$$v_{i,m} = Rv_{i,m-1} + Q\hat{v}_{i,m} \tag{24}$$

where R is the one-time-step autocorrelation of v, $Q = (1 - R^2)^{1/2}$, and $\hat{v}_{im}$ is randomly chosen from a Gaussian distribution with variance $\overline{v^2}$. First-order Markov chains of the type in (24) now have an extensive literature with applications to turbulent dispersion and have appeared with various key words such as "random walk", "Monte-Carlo", "Langevin equation", "random flight" (Durbin 1980), etc. A recent example in oceanography, where some of the history of this method is presented and where a partial justification of (24) for the simulation of turbulent fluid flow is advanced, is that of Rahm and Svennson (1986).

The forward time step

$$y_{i,m+1} = y_{i,m} + (\tilde{v}(y_{i,m}) + v_{i,m})\Delta t \tag{25}$$

advances the tracer. Each tracer is treated independently, and in this application we imagine the tracers to be strung out in x so that tracers with the same y_m are advected by the same $\tilde{v}$ but are not influenced by the same turbulent eddies.

The value of R is frequently determined from $R = \exp(-\Delta t/T_l)$, where Δt is the time step, but it is shown in appendix B that with the combination of (24) and (25) and with no gradient of the mean flow, at large t the tracer variance is given exactly by using

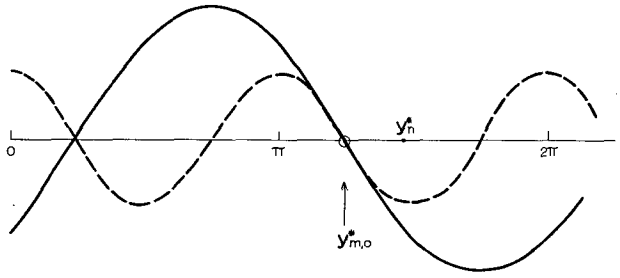

FIG. 6. The phase relation between one of the primary sinusoidal components of the surface flow (solid line) and its harmonic (dashed line). The convergence lines coincide at $y^*_{n,0}$ (see appendix B). $y^*_{n,0}$ changes with time as the cells move laterally and is different for each of the three components; y^* is the position of some tracer.

$$R = (2 - \Delta t/T_t)/(2 + \Delta t/T_t) \qquad (26)$$

for all $\Delta t \leqslant 2T_t$, and therefore (26) is preferable to the exponential form which is correct only to second order in $\Delta t/T_t$. At $\Delta t = 2T_t$, $R = 0$ and $v_{im} = \hat{v}_{i,m}$, a random walk. Therefore in suitably simple circumstances a random walk can be used for each tracer provided $\Delta t = 2T_t$.

When convergent mean flows are present, however, (26) can no longer give exact results. The modification of (26) for uniformly convergent flow involves the parameter T_t^* and will be given in a separate publication. With variable convergence higher derivatives of $\tilde{v}$ should also be taken into account but no such corrections have as yet been devised. Approximately correct results can be obtained using (26) or with the exponential form, however, if a sufficiently small value of $\Delta t/T_t$ is used.

Random-flight calculations require that the turbulence be specified by at least $\overline{v^2}$ and T_t. If the turbulence is inhomogeneous or nonisotopic much more information is required and the computational methods are elaborate. An apparently successful method has been developed for spatial variations of $\overline{v^2}$ (e.g., Thompson 1984; van Dop et al. 1985) but their methods cannot be applied here, and in all of the following random-flight calculations we have treated only homogeneous, isotopic turbulence.

5. Time-dependent, spatially irregular cells

Here the LCs remain independent of x but have time-dependent amplitudes and phases, and a more complicated structure in y is introduced. Our original time-dependent cell calculations (Auer 1985) represented cells in y and z and included the dispersion of internal tracers of various specific gravities. But here we limit our discussion to computations of the lateral dispersion of surface tracers.

The mean surface flow was assumed to be

$$\tilde{v} = Vk \sum_{n=1}^{3} \left(\frac{A_n}{k_n} \sin k_n y + \frac{B_n}{k_n} \cos k_n y + \frac{A'_n}{2k_n} \sin 2k_n y + \frac{B'_n}{2k_n} \cos 2k_n y \right) \qquad (27)$$

where the A'_n and B'_n are related to A_n and B_n as described in appendix C and as shown in Fig. 6. Thus $\tilde{v}$ was that due to the sum of three primary sinusoidal cells plus first harmonics. The primary wavenumbers were $k_1 = k$, $k_2 = 3k/4$ and $k_3 = 4k/3$. The amplitudes A_n and B_n were time-dependent, and each was independently determined by a recursion relation analogous to (24), namely

$$X_m = R_C X_{m-1} + Q_C \hat{X}_m \qquad (28)$$

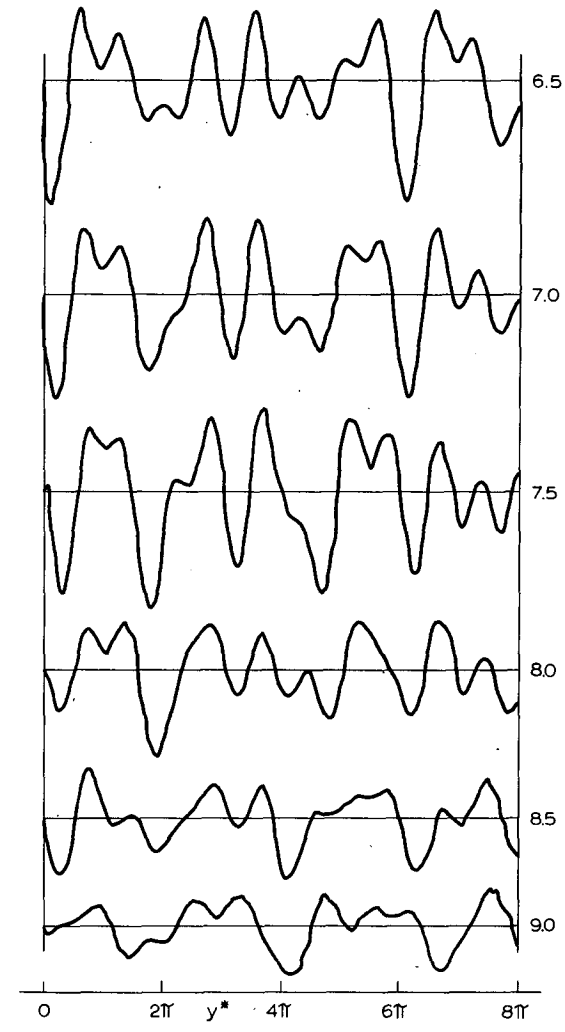

FIG. 7. An example of the time evolution of the surface flow $\tilde{v}$ from Eq. (27). The number of time scales T_t^* is indicated at the right.

where

$$R_C = (2 - \Delta t/T_C)/(2 + \Delta t/T_C),$$
$$Q_C = (1 - R_C^2)^{1/2}, \quad (29)$$

and $\hat{X}_m$ was randomly selected from a Gaussian distribution with variance $X^2 = 0.133V^2$. This coefficient guaranteed that the time–space average of $\tilde{v}^2$ would be $V^2/2$, the same variance as for a single sine wave with amplitude V. Figure 7 illustrates a typical time–space variation of $\tilde{v}$ from (27). There one sees large changes of amplitude and phase, and an obvious effect of the harmonics as well.

Equation (27), although arbitrary, allowed the lateral drift of cells and changes of the relative amplitudes of the three basic components, all with the time scale T_C. It also provided an instantaneous spatial variability of the cell scales and speeds that might be expected in natural circumstances due to stochastic variations of the wind or other disturbing factors. It is believed, therefore, that surface dispersion calculated with this version of $\tilde{v}$ is reasonably representative of natural conditions except for effects attributable to the downwind variation of the cells that is frequently observed. This latter effect is added in section 6.

To minimize computations while obtaining meaningful statistics on the large-scale dispersion, each tracer was started from $y = 0$ but a different sequence of randomly selected amplitudes was applied to each tracer. This procedure avoided the necessity of having to wait excessively long computational times, which would have been necessary for representative results with a coherent cloud of tracers. Thus if all tracers were subject to the same cellular motions, as in the examples of Fig. 8, one would have to integrate for many T_C for statistical significance.

The computed random-flight dispersion results are most conveniently represented in terms of non-dimensional parameters. The independent variates spanned the ranges $0 \leqslant v^* \leqslant 3.2$ and $1 \leqslant T_c^* \leqslant 80$ while T_l^* was kept at 0.1. This latter value is representative of natural conditions and is small enough that its specific value has little effect except as it enters $D^* = v^{*2}T_l^*$. Thus with fixed T_l^*, the value of v^* is itself a measure of the small-scale turbulent diffusion.

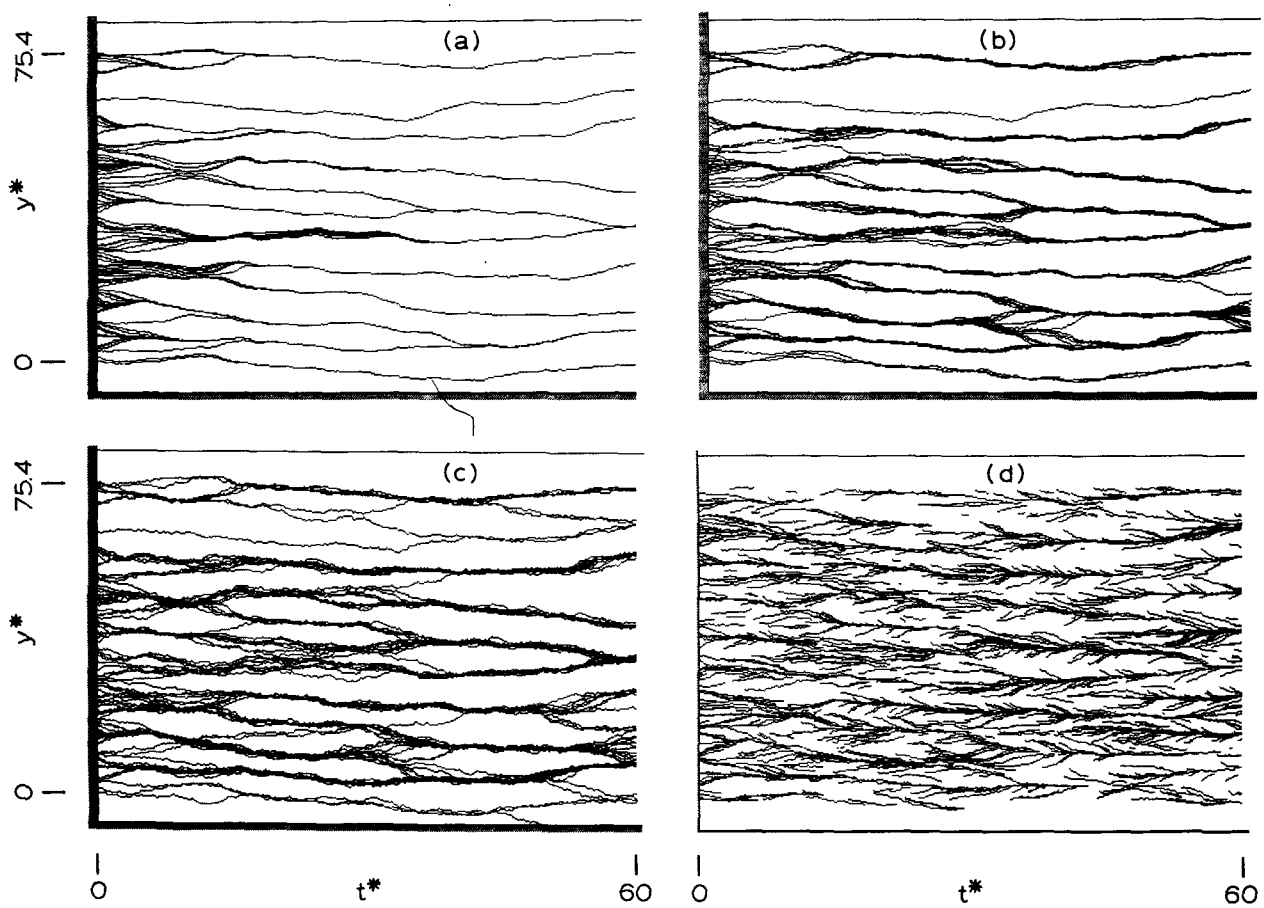

FIG. 8. Trajectories of 100 tracers calculated from the random-flight model of (27). All panels have the same time-dependent cells and are for $T_c^* = 10$; (a), (b) and (c) are for $v^* = 0$, 0.4 and 0.8, respectively, and the tracers are randomly distributed in the interval $0 < y^* < 75.4$ at $t^* = 0$. (d) The tracers are introduced randomly in time and space and have an average lifetime of $\delta t^* = 5$.

TABLE 2. Dispersion coefficients, K^*, from random-flight computations with time-dependent cells having phase-locked harmonics. Upper: K^* as dependent upon v^* and T_C^* with $T_t^* = 0.1$. Bottom: The corresponding ratios K^*/D^* as dependent upon D^* and T_C^*. Statistical uncertainties for K^* are typically 3 to 10 percent for one standard deviation of the given means. The boxed value denotes our standard oceanic conditions. The dashed line encloses most conditions to be expected in nature.

	T_C^*						
v^*	1.0	2.5	5.0	10.0	20.0	40.0	80.0
0	0.192	0.200	0.150		0.071	0.037	
0.2		0.206	0.172	0.114	0.072		
0.4	0.214	0.213	0.161	0.107	[0.077]	0.059	0.017
0.8	0.241	0.224	0.175	0.130	0.095	0.050	0.026
1.6		0.342			0.143		0.057
3.2	1.193	0.965	0.885	0.869			0.485
D^*							
0	∞	∞	∞	∞	∞	∞	∞
0.004		52	43		29	18	
0.016	13	13	10	7	[5]	3.7	1.1
0.064	3.8	3.5	2.7	2.0	1.5	0.8	0.4
0.256		1.34			0.56		0.22
1.024	1.17	0.94	0.86	0.85			0.42

The maximum allowable time step $\Delta t^* = 2T_t^* = 0.2$ was used, and thus the turbulence was treated as a random walk while at the same time $\Delta t^*/T_C^*$ was generally small. Nevertheless, to obtain reasonable accuracy each advective step was iterated so as to use the average of $\tilde{v}$ at the beginning and end of each displacement. Occasional checks with shorter time steps showed little differences in the computed values of the significant dependent variate, $K^* \equiv KV/k$. In each calculation the displacements of 1000 tracers were calculated for nondimensional time intervals ranging from 80 to 160.

Table 2 presents the calculated values of K^* and the ratios K^*/D^* for wide ranges of v^* and T_C^*. For $K^*/D^* < 1$ the cells inhibit dispension. The trends of K^* with v^* and T^* are as should be expected. Up to the value 0.8, v^* has little influence on K^* as long as $T_C^* < 40$ because dispersion is then dominated by the time-dependent wandering of the cells and rows. This is the region of the table where $K^*/D^* > 2$. As v^* increases above 0.8 and as T_C^* increases, the turbulence has a more noticeable effect. Note that at the highest value $v^* = 3.2$ ($D^* = 1.024$) the cells inhibit dispersion ($K^*/D^* < 1$) when $T_C^* > 1$ even though they are time-dependent.

Our standard oceanic conditions (section 2) are shown in Table 2 by the boxed values, and the dashed line is meant to suggest that probably all natural conditions fall within this region, the steady parallel streak conditions lying at large T_C^*. For very rapidly changing cells, i.e., below $T_C^* = 1$, sample computations (not tabulated) show decreasing K^* because the cells lose their strong advective effect and act only to augment the turbulence. Thus, the maximum dispersive effect occurs when $T_t^* = O(1)$ as might be expected.

In the vicinity of our standard conditions K^* varies as $T_C^{*-1/2}$. This dependence upon T_C^* is quite different from the T_C^{*-1} dependence of the Csanady (1974) row-splitting model. In an attempt to understand this difference the complex model of (27) was simplified in steps to the single-wave, fixed-phase model

$$\tilde{v} = A(t) \sin y^*. \tag{30}$$

The values of $K^*(T_C^*)$ in Table 3 were obtained by the random-flight method with $v^* = 0.4$ and using (30) for the prescribed flow. The resultant K^* of Table 3 are remarkably close to the values of Table 2, considering the simplifications, and still show $K^* \approx T_C^{*-1/2}$.

The similar results from (27) and (30) are a consequence of two counter-balancing effects. On the one hand the simpler model does not have the continuous cell wandering effect that characterizes the complex model. But there are abrupt 180 degree phase changes when $A(t)$ changes sign. At such a change each well-developed row is suddenly found to be directly over a divergence line and row splitting begins. Thus row splitting is the sole mechanism of dispersion for the simpler model, excepting the negligible direct effect of

TABLE 3. Values of K^* from random-flight calculations for time-dependent cells represented by a single sine wave and for a wide range of T_C^*. The other parameters were fixed at $v^* = 0.4$ and $T_C^* = 0.1$, hence $D^* = 0.016$. Near oceanic conditions ($T_C^* = 20$), $K^* \propto (T_C^*)^{-1/2}$. Uncertainties are 1 standard deviation of the mean.

T_C^*	K^*
0.125	.0533 ± .0027
0.250	.0779 ± .0048
0.50	.1137 ± .0065
1.0	.1524 ± .0067
2.5	.1805 ± .0083
5	.1408 ± .0072
10	.1072 ± .0051
20	.0866 ± .0064
40	.0551 ± .0081
80	.0384 ± .0018
160	.0228 ± .0014

turbulence. But row splitting takes time and sometimes $A(t)$ changes back and restores the original row before splitting has been completed, and the parameters v, V and T_C all play a role in this question.

An extended analysis of this process suggests that the $T_C^{*-1/2}$ effect for the simpler model is related to the finite time required for row splitting in relation to T_C, an effect not present in the Csanady model. From the complex model based upon (27) and the simpler model based upon (30) we conclude that both row wandering and row splitting lead to $K^* \approx T_C^{*-1/2}$.

Figure 8 illustrates simulated $t^* - y^*$ trajectories based upon (27). 100 tracers were released randomly in the interval $0 < y^* < 75.4$ at $t^* = 0$. (This interval, $12 \times 2\pi$, is the smallest range of y^* that includes integral multiples of the 3 assigned wavelengths). The same sequence of random numbers was used to generate the cell amplitudes, hence all the patterns of Fig. 8 are similar.

Panels (a)–(c) of Fig. 8 differ only by the values $v^* = 0$, 0.4 and 0.8, respectively. Panel (d) is for $v^* = 0.4$ but the tracers are introduced randomly in time, as well as in y^*, and have a finite lifetime, Δt^*, randomly selected from the interval $0 < \Delta t^* < 10$. Thus panel (d) illustrates how tracers with different characteristics may present rather different patterns in the same cells. Following this line of thought one should not interpret any of these patterns as being analogous to instantaneous patterns of tracers on the ocean surface.

Panels (a)–(c) show increased row width and increased row splitting for large v^*, but in general the row splitting is overcome by row merging and a reduction of the number of rows with time. Over a much longer time, however, as the whole pattern spreads, one might expect the eventual appearance of many more rows. In panels (a)–(c) it is not obvious from the appearance of the rows that there has been any tracer dispersion at all, but in fact the nondimensional dispersion coefficients, computed from $\overline{\Delta y^{*2}}/2\Delta t^*$ and from $t^* = 10$ to $t^* = 60$, were $K^* = 0.44$, 0.45 and 0.40 in (a), (b) and (c), respectively. These values are about four times the corresponding values from Table 2 and are not at all good estimates of an average K^* for these conditions. The above values suffer from: 1) a small sample of tracers, 2) a short time, and 3) the fact that of all 100 tracers only 5 to 10 can be considered to be independent because all tracers are imbedded in the same cellular pattern and group into only a few rows.

In dimensional terms and based upon our standard conditions the band of tracers is 452 m wide, the time of observation is 60 min, and the dispersivity is about $K = 0.25\ \mathrm{m^2\ s^{-1}}$. These model results suggest that the determination of a representative value of K on the ocean by following surface tracers will be at best a tedious task.

The row widths in panels (b) and (c) of Fig. 8 are in general agreement with (19) and with Table 1, but precise values cannot be obtained from the figure.

The time-dependent-cell model as developed in this section has cells independent of x. But if we assume that all tracers move downwind in rows (along x) at some fixed speed U_w^*, the t^* coordinate in Fig. 8 can be converted to x^*. For $U_w^* = 3$ and for our other standard values the abscissa would correspond to a length of 1080 m. This representation will be considered further in section 6 where an x-dependence of the cells is introduced.

6. Downwind dependence of the cells

When LCs have a significant time dependence, presumably because of fluctuating winds, it seems likely that they also will be x-dependent more or less in proportion to their t-dependence. Therefore, we now assume that the joint t- and x-dependence can be represented by

$$A_n \approx \exp(-t/T_c)\exp(-x/X_c) \tag{31}$$

where A_n is the amplitude of some cellular component in (27) and X_c is a characteristic length scale of the cells along x. Now letting $x = U_w t$, where U_w is a fixed speed of tracers in the windrows, we define T_A, an advective time scale, as

$$T_A = X_C/U_w. \tag{32}$$

Then (31) becomes

$$A_n \approx \exp(-t/T_B) \tag{33}$$

where T_B is the harmonic mean

$$T_B = \frac{T_A T_c}{T_A + T_c}. \tag{34}$$

As a specific example, and perhaps a case typical of oceanic conditions, take $X_c = mL$ and $m = 10$. Then using $U_w = 0.3\ \mathrm{m\ s^{-1}}$ and $T_c = L/(0.03\ \mathrm{m\ s^{-1}})$ it is found that $T_A = T_c$ and therefore

$$T_B = T_c/2. \tag{35}$$

In such a case both the t- and x-dependence of the cells are taken into account simply by using $T_B^* = T_c^*/2$ in place of T_c^* in Table 2. Then for $T_c^* = 20$, $T_B^* = 10$, and it was for this reason that the plots of Fig. 8 were based upon $T_c^* = 10$. The abscissa of Fig. 8 can now be interpreted as x^* and the plots can be thought of as representing results for $T_c^* = T_A^* = 20$. The curves then represent $x^* - y^*$ Lagrangian trajectories.

Continuing in this vein, for $T_c^* = 20$ and $v^* = 0.4$ we may enter Table 2 with $T_B^* = 10$ (to account for the x dependence) and find $K^* = 0.107$. Then, within the uncertainty of Table 2

$$K^* = 0.35T_B^{*-1/2} = 0.5T_c^{*-1/2}, \tag{36}$$

a specific model prediction for comparison with oceanic data that we may hope to obtain in the future.

It also may be considered desirable to represent the large-scale dispersion by

$$K_L = V_L^2 T_L \quad \text{or} \quad K_L^* = V_L^{*2} T_L^* \tag{37}$$

where V_L and T_L are appropriate Lagrangian velocity and time scales for displacements in y when all effects of the turbulence and the cells have been included. But it is not a simple matter to propose a formulation of either V_L or T_L because of the several velocity and time scales that must be involved. The V_L must be a composite of the effects of V, v and $(kT_c)^{-1}$ (a cell-wandering speed) and T_L must represent the effects of T_t, T_c and $(kV)^{-1}$. In particular a simple relation such as $V_L = V^\alpha v^\beta (kT)^{-\gamma} (\alpha + \beta + \gamma = 1)$ cannot succeed inasmuch as Table 2 shows that for $v^* = 0$ there is still a finite value of K^* and therefore a nonzero V_L^*. Values of V_L^* and T_L^* can be calculated from the random-flight model of section 5, however, and for the case $T_B^* = 10$ and $v^* = 0.4$ a sample calculation gave $T_L^* = 0.38$ and $V_L^{*2} = 0.29$. A second calculation at $T_B^* = 10$, but for $v^* = 0$, gave $T_L^* = 1.51$ and $V_L^{*2} = 0.09$. Thus these values are quite sensitive to the level of v^* even though the small-scale turbulence plays only a small role in the dispersion.

The observations necessary to test the dependence of K^* upon T_c^*, as in (36), and to determine the proportionality factor might be obtained by scattering many sheets of paper from a helicopter and then determining their individual and collective motions by photogrammetry. Measurements of V would require frequent photos within the first 2–3 min after the papers landed, i.e., before they lined up in rows. The immediate determination of tracer motions would also allow an estimate of the average surface flow along and to the right of the wind, values that become highly biased once the tracers find the windrows. Instrumented anchored buoys could provide reference markers and the necessary environmental data. Estimates of the turbulence could be obtained from the tracer motions, as could V_L and T_L, and turbulence could also be estimated from the width of windrows as in section 2. Such measurements could materially enhance our knowledge of Langmuir circulations and their role in the mixed layer.

7. Summary and conclusions

We have presented a series of dispersion models designed to simulate the probable roles of Langmuir circulations on the dispersion of surface tracers in lakes and oceans. A second objective is to learn as much as possible about mixed-layer processes by a comparison of these models with the directly observable motions of surface tracers that may be obtained in future observational studies. We hasten to add that rolls produced by thermal convection or by Ekman layer instability will have the same scales of motion and the same kinematic effects as the larger LCs.

Some significant model results and conclusions are:

1) Small scale turbulence has only a negligible effect upon lateral surface dispersion when LCs are present. Steady, parallel LCs concentrate floating tracers into lines, completely dominating any dispersive effect of the turbulence. With t- and x-dependent LCs the small-scale turbulence may slightly enhance dispersion by causing wider windrows and thus increasing the probability of row splitting by the time dependence of the cells and by downwind advection of the tracers.

2) The widths of windrows of discrete tracers can be used to estimate the relative strengths of the cellular circulations and the surface turbulence by using (19), provided that surface films do not seriously affect the tracer motions.

3) The random-flight model, with parameters representative of the ocean, indicates that stochastic variations of the LCs in t and in x, and the associated wandering of the windrows, is the principal mechanism of dispersion. Row splitting occurs occasionally but the width of the rows is usually too small for frequent splitting. This conclusion is based upon the results in Table 2, namely that the turbulence parameter v^*, which in part governs the row width, has only a small influence upon K^* in the range of our standard conditions.

4) The random-flight model has led to the explicit prediction $K^* = 0.5\ T^{*-1/2}$ for variable wind conditions. The dependence of K^* upon $T_C^{*-1/2}$ (rather than upon T_C^{*-1}, as in the Csanady (1974) row-splitting model) has been tested with several variations of the model of section 5 and appears to be robust for the oceanic range of parameters.

5) Model results for a wide range of conditions other than our standard values can be obtained from the nondimensional results in Table 2. In dimensional terms and in the vicinity of our standard values the dispersion coefficient is $K = 0.5(V/k^3 T_C)^{1/2}$, and for our specific standard values one obtains $K = 0.067\ \text{m}^2\ \text{s}^{-1}$, approximately 5 times the assumed turbulent diffusivity, D.

Because of the importance of LCs in mixed-layer dynamics, we believe that detailed observations of the motions of surface tracers on lakes and oceans under a wide variety of circumstances would be an efficient and inexpensive way of determining the effects of LCs under various weather and water conditions. The theories and models presented here can provide a guide to the conduct of such experiments in our efforts to find out what mixed layer processes are really like and how they respond to the wide variety of forcing conditions that are found in nature.

Acknowledgments. This research was supported in part by the National Science Foundation under Grant ATM 3217139 and in part by the Computer Science Center of the University of Maryland. It was initiated while Mr. Auer was on leave under the NOAA Graduate Scientist Program, and it is OPC Contribution Number 15.

APPENDIX A

The Time Scales T_R and T_c

In the time-dependent-cell model of section 5 we introduce a cell time scale, T_c, that characterizes the changing amplitudes and phases of the cells. This should not be confused with the overturning time scale, $T_v = (Vk)^{-1}$. For natural processes the corresponding T_c might be the correlation time scale of the crosswind component of the surface flow, or a temporal pattern correlation time scale, all with respect to some defined point moving with some average speed of the mixed layer. For the convenience of theory and computation we assume that temporal correlations of $v(x, y, t)$ are of the form $\exp(-t/T_c)$.

For the time-dependent-cell model of section 5 we require a typical value of T_c to accompany a typical value of L for the ocean. Nearly steady cells with very large values of T_c may occur in the oceans for stable wind conditions. But for gusty winds it seems likely, as argued below, that T_c will be closely related to the natural response time for the generation of cells, T_R. And because of the inertia of larger cells we should expect T_R to be a monotonically increasing function of the cell scale, L.

Assume a linear model for the growth of cells

$$M\frac{dV}{dt} = F(t) - bV \tag{A1}$$

where V is a representative speed, $M \approx L^2$ is the mass per unit length of fluid accelerated, $F(t)$ is a prescribed forcing, and b is a linear damping coefficient. With $F = F_0 \cos(\omega t)$ the solution of (A1) is

$$V = \frac{F_0}{M}(b' \cos\omega t + \omega \sin\omega t - b' \exp(-b't))/(b'^2 + \omega^2) \tag{A2}$$

where $b' = b/M$. Equation (A2) illustrates the exponential transient response at small t and the periodic long term response.

For steady forcing (i.e., $\omega \to 0$) (A2) reduces to

$$V = F_0 b^{-1}(1 - \exp(-b't)) \tag{A3}$$

and it is apparent that the response time is

$$T_R \equiv b'^{-1} = M/b. \tag{A4}$$

Stochastic forcing can be represented by

$$F(t) = \sum_{n=0}^{\infty} F_n \cos\omega_n t, \tag{A5}$$

and by the linearity of (A1) the solutions for each n can be added. Then it is apparent from (A2) that for $\omega_n^2 > b'^2$ the corresponding amplitudes will be relatively small. Then if F_n is more or less independent of n, T_R will be not only the response time but the cutoff time scale below which there is little energy in the cells. Therefore, one should typically expect to find observed time scales satisfying

$$T_c \geqslant T_R, \tag{A6}$$

and T_R is, in effect, a minimal T_c.

Now note that whereas $T_R = M/b$ and $M \approx L^2$, if we assume that $b \approx L$ we obtain $T_R \approx L$, a result that is also suggested by observations shown in Fig. 3. The assumption $b \approx L$ is not unreasonable if one imagines that large cells are accompanied by large eddy viscosity.

The available observations of the time dependence of LCs all relate to the response time T_R. Langmuir (1938) reported that windrows of *Sargassum* with L = O(100 m) reoriented within 20 min due to a shift of wind direction. Stommel (1952) reported that an analysis of film streaks from several small ponds under generally gusty wind conditions showed that the streaks quickly reoriented after a shift of wind direction "in 1 or 2 minutes", say 100 s. Spacings were not reported, but from similar experiences of the authors, spacing of 2–3 m would be appropriate. Welander (1963) reported that a streak spacing of 8 m reoriented with an abrupt wind shift within about 10 min. Faller and Cartwright (1983) measured the rate of growth of LCs having a predetermined wavelength of 44 cm in a laboratory tank and found characteristic time scales for their growth of 2.6, 12 and 15 s (nominally 10 s), the value of T_C increasing with the wind speed. Finally Faller and Caponi (1978, Fig. 6) found that for wind-generated cells: in water of average depth 5.5 cm the initial cells had an average spacing of about 6.2 cm and they first became evident in dye at the bottom of the tank at an average time of about 22 s after they began to form. This collection (Fig. 3) spans a large range of L, but it is neither of sufficient uniformity nor accuracy to support other than a simple linear relation and, therefore, we adopt the relation $T_R = L/(0.03 \text{ m s}^{-1})$.

To proceed with a time-dependent model it is nec-

essary to have a value of T_C, and so we assume that $T_C = L/(0.03 \text{ m s}^{-1})$ thus implying that our model refers to somewhat irregular wind conditions.

APPENDIX B

Random-flight Calculations

Starting with

$$v_{im} = Rv_{i,m-1} + Q\hat{v}_{i,m} \tag{B1}$$

and

$$y_{i,m+1} = y_{i,m} + v_{i,m}\Delta t \tag{B2}$$

we seek an expression for R such that at large $t = m\Delta t$ the variance $\overline{y_{i,m}^2}$ for an infinite ensemble (represented by the bar) is the same as the corresponding analytically derived variance, $y^2(t)$, where $t = m\Delta t$.

Combining (B1) and (B2), after four time steps the displacement of a tracer (dropping subscript i) is

$$y_4 = y_0 + \Delta t[(1 + R + R^2 + R^3)v_0 + Q((1 + R + R^2)\hat{v}_1 + (1 + R)\hat{v}_2 + \hat{v}_3)]. \tag{B3}$$

The mean square value of y_4 is then

$$\overline{y_4^2} = \overline{y_0^2} + \Delta t^2\overline{v^2}(4 + 6R + 4R^2 + 2R^3) \tag{B4}$$

having used the relations $\overline{\hat{v}_m^2} = \overline{v_0^2} = \overline{v^2}$, $\overline{\hat{v}_j\hat{v}_k} = 0$, $j \neq k$, and $Q^2 = 1 - R^2$; and having assumed no linear relation between v_0 and y_0.

An examination of expressions like (B4) for several time steps shows that for m steps

$$\overline{y_m^2} = \overline{y_0^2} + \Delta t^2\overline{v^2}[m + 2((m - 1)R + (m - 2)R^2 + \cdots (m - (m - 1))R^{n-1})]. \tag{B5}$$

For large m (B5) reduces to simply

$$\overline{y_m^2} = \overline{y_0^2} + \Delta t^2\overline{v^2}m(1 + R)/(1 - R). \tag{B6}$$

The corresponding large-time theoretical solution for continuous diffusion, following Taylor (1921) is

$$\overline{y^2}(t) = \overline{y^2}(0) + 2\overline{v^2}T_t t. \tag{B7}$$

Comparing (B6) and (B7) using $t = m\Delta t$ one obtains

$$R = (2 - \Delta t/T_t)/(2 + \Delta t/T_t). \tag{B8}$$

Random-flight calculations of dispersion in homogeneous turbulence have confirmed that (B8) is correct up to $\Delta t/T_t = 2$. This formulation, however, does not preserve higher moments of the tracer distribution and therefore should be used with caution.

APPENDIX C

Harmonic Phase Relations

It is well known from a variety of field observations, laboratory experiments, and theory that LCs have concentrated strong downwelling and broad weak upwelling. To properly represent the corresponding asymmetry in the surface flow would require a large number of harmonics of the basic sinusoidal variation of $\tilde{v}$, but for practical computational reasons we have included only a first harmonic of each basic component in (27).

Our computed convergence lines drift laterally due to the stochastic nature of A_n and B_n, and to maintain concentrated downwellings the harmonic amplitudes A'_n and B'_n in (27) must change in such a way as to keep a convergence line of each harmonic coincident with a convergence line of each primary wave (Fig. 6).

Algorithms to directly determine A'_n and B'_n are unnecessarily complex and computations are minimized by the use of

$$\tilde{v}_n^* = -D_n(\sin\Delta y_n + 0.5 \sin 2\Delta y_n) \tag{C1}$$

in place of (27). In (C1) $D_n = (A_n^2 + B_n^2)^{1/2}$, $\Delta y_n = y_n^* - y_{n0}^*$, $y_n^* = k_n y/k$, $y_{n,0}^* = \tan^{-1}(A_n/B_n) + \pi/2$ and $y_{n,0}^* \rightarrow y_{n,0}^* + \pi$ if $B_n < 0$. Equation (C1) is applied to each component n and the total mean flow is $\tilde{v}^* = \tilde{v}_1^* + \tilde{v}_2^* + \tilde{v}_3^*$.

REFERENCES

Assaf, G., R. Gerard and A. L. Gordon, 1971: Some mechanisms of oceanic mixing revealed in photographs. *J. Geophys. Res.*, **76**, 6550–6572.

Auer, S. J., 1985: The effects of Langmuir circulation on lateral turbulent dispersion in the mixed layer. M.S. thesis, Dept. of Meteor., University of Maryland.

Buranathanitt, T., and D. J. Cockrell, 1979: Some effects of Langmuir circulation on suspended particles in lakes and reservoirs. Rep. 79-6, Dept. of Eng., University of Leicester.

Cowen, R. C., 1960: *Frontiers of the Sea.* Doubleday, 307 pp.

Craik, A. D. D., 1977: The generation of Langmuir circulations by an instability mechanism. *J. Fluid Mech.*, **81**, 209–223.

——, and S. Leibovich, 1976: A rational model for Langmuir circulations. *J. Fluid Mech.*, **73**, 401–426.

Csanady, G. T., 1970: Dispersal of effluents in the Great Lakes. *Water Res.*, **4**, 79–114.

——, 1974: Turbulent diffusion and beach deposition of floating pollutants. *Advances in Geophysics*, Vol. 18A, Academic Press, 371–381.

Das, A. K., 1979: Stochastic diffusion in a periodic potential. *Physica*, **98A**, 528–544.

Durbin, P. A., 1980: A random flight model of inhomogeneous turbulent dispersion. *Phys. Fluids*, **23**, 2151–2153.

Faller, A. J., 1969: The generation of Langmuir circulations by the eddy pressure of surface waves. *Limnol. Oceanogr.*, **14**, 504–513.

——, 1978: Experiments with controlled Langmuir circulations. *Science*, **201**, 618–620.

——, and A. H. Woodcock, 1964: The spacing of windrows of Sargassum in the ocean. *J. Mar. Res.*, **22**, 22–29.

——, and E. A. Caponi, 1978: Laboratory studies of wind-driven Langmuir circulations. *J. Geophys. Res.*, **83**, 3617–3633.

——, and P. C. Mignerey, 1982: One-dimensional turbulent dispersions in convergent and divergent flows. *Phys. Fluids*, **25**, 1306–1316.

——, and R. W. Cartwright, 1983: Laboratory studies of Langmuir circulations. *J. Phys. Ocean.*, **13**, 329–340.

——, and C. Perini, 1984: The roles of Langmuir circulations in gas transfer across natural water surfaces. *Gas Transfer at Water Surfaces*, Brutsaert and Jirka, Eds. Reidel, 639 pp.

——, and A. J. Auer, 1987: The roles of Langmuir circulations in the dispersion of surface tracers. Tech. Note BN 1058, Institute

for Physical Science and Technology, University of Maryland, College Park, MD, 20742.

Filatov, N. N., S. V. Rjanzhin and S. V. Zaycev, 1981: Investigation of turbulence and Langmuir circulation in Lake Ladoga. *J. Great Lakes Res.*, **7**, 1–6.

Johnson, D. L., and P. L. Richardson, 1977: On the wind-induced sinking of Sargassum. *J. Exp. Mar. Biol. Ecol.*, **28**, 255–267.

Kenney, B. C., 1977: An experimental investigation of the fluctuating currents responsible for the generation of windrows. Ph.D. thesis, University of Waterloo, 163 pp.

Langmuir, I., 1938: Surface motion of water induced by wind. *Science*, **87**, 119–123.

Leibovich, S., 1983: The flow and dynamics of Langmuir circulations. *Ann. Rev. Fluid Mech.*, **15**, 000–000.

——, and S. Paolucci, 1980: The Langmuir circulation instability as a mixing mechanism in the upper ocean. *J. Phys. Oceanogr.*, **10**, 186–207.

McLeish, W., 1968: On the mechanisms of wind-slick generation. *Deep-Sea Res.*, **15**, 461–469.

Myer, G. E., 1971: Structure and mechanics of Langmuir circulations on a small inland lake. Ph.D. dissertation, State University of New York, Albany, 107 pp.

Neumann, G., and W. J. Pierson, 1966: *Principles of Physical Oceanography*, Prentice-Hall, 545 pp.

Okubo, A., 1971: Oceanic diffusion diagrams. *Deep-Sea-Res.*, **18**, 789–802.

Rahm, L.-A., and V. Svennson, 1986: Dispersion of marked fluid elements in a turbulent Ekman layer. *J. Phys. Oceanogr.*, **16**, 2084–2096.

Richardson, L. F., 1926: Atmospheric diffusion shown on a distance-neighbor graph. *Proc. Roy. Soc. London*, **110A**, 709–737.

Ryter, D., 1982: Renormalized diffusion in systems with periodic variables. *Z. Phys., B-Condensed Matter*, **49**, 63–68.

Scott, J. T., G. E. Meyer, R. Stewart and E. G. Walther, 1969: On the mechanism of Langmuir circulations and their roll in epilimnion mixing. *Limnol. Oceanogr.*, **14**, 493–503.

Smith, J., R. Pinkel and R. A. Weller, 1987: Velocity structure in the mixed layer during MILDEX. *J. Phys. Oceanogr.*, **00**, 000–000.

Stommel, H., 1951: Streaks on natural water surfaces. *Weather*, **6**, 72–74.

——, 1952: Streaks on natural water surfaces. Geophys. Res. Papers No. 19, Geophysics Res. Directorate, Air Force Cambridge Res. Center, 145–154.

Sutcliffe, W. H., E. R. Baylor and D. W. Menzel, 1963: Sea surface chemistry and Langmuir circulation. *Deep-Sea Res.*, **10**, 233–243.

Taylor, G. I., 1921: Diffusion by continuous movements. *Proc. London Math. Soc.*, **A20**, 196–211.

Thompson, D. J., 1984: Random walk modelling of diffusion in inhomogeneous turbulence. *Quart. J. Roy. Meteor. Soc.*, **110**, 1107–1120.

van Dop, H., F. T. M. Nieuwstadt and J. C. R. Hunt, 1985: Random walk models for particle displacements in inhomogeneous unsteady turbulent flows. *Phys. Fluids*, **28**, 1639–1653.

Weaver, D. L., 1979: Effective diffusion coefficient of a Brownian particle in a periodic potential. *Phys.*, **98A**, 339–362.

Welander, P., 1963: On the generation of wind streaks on the sea surface by action of surface film. *Tellus*, **15**, 1–5.

Weller, R. A., J. P. Dean, J. Marra, J. F. Price, E. A. Francis and D. C. Boardman, 1985: Three-dimensional flow in the upper ocean. *Science*, **227**, 1552–1556.

Williams, K. C., 1965: Turbulent water flow patterns resulting from wind stress on the ocean. Mem. Rep. 1653, U.S. Naval Res. Lab., Washington, D.C.

Woodcock, A. H., 1950: Subsurface pelagic Sargassum. *J. Mar. Res.*, **9**, 77–92.